

# A cesium copper vanadyl-diphosphate: Synthesis, crystal structure and physical properties



Larisa Shvanskaya <sup>a,c,\*</sup>, Olga Yakubovich <sup>a</sup>, Andrey Bychkov <sup>a</sup>, Vasiliy Shcherbakov <sup>a</sup>, Alexey Golovanov <sup>b</sup>, Elena Zvereva <sup>b</sup>, Olga Volkova <sup>b,d</sup>, Alexander Vasiliev <sup>b,c,d</sup>

<sup>a</sup> Geology Faculty, M.V. Lomonosov Moscow State University, Moscow 119991, Russia

<sup>b</sup> Physics Faculty, M.V. Lomonosov Moscow State University, Moscow 119991, Russia

<sup>c</sup> National University of Science and Technology "MISiS", Moscow 119049, Russia

<sup>d</sup> Theoretical Physics and Applied Mathematics Department, Ural Federal University, 620002 Ekaterinburg, Russia

## ARTICLE INFO

### Article history:

Received 17 September 2014

Received in revised form

24 October 2014

Accepted 2 November 2014

Available online 11 November 2014

### Keywords:

Complex metal phosphate

High-temperature crystallization

Crystal structure

Structural disorder

Physical properties

## ABSTRACT

A non-centrosymmetric orthorhombic diphosphate,  $Cs_2Cu_{1+x}(VO)_{2-x}(P_2O_7)_2$  ( $x=0.1$ ) with  $a=13.7364$  (2) Å,  $b=9.2666(2)$  Å,  $c=11.5678(2)$  Å,  $Z=4$ , has been isolated. Its 3D framework is built from Cu atoms in square pyramidal and square planar coordination,  $VO_5$  tetragonal pyramids and  $P_2O_7$  diphosphate groups, sharing vertices. Large channels are fulfilled by cesium atoms. The ESR study reveals a similarity in behaviour of two paramagnetic (Cu and V) subsystems. The temperature dependences of the ESR linewidth and static magnetic susceptibility data present evidences for a cluster type magnetic ordering in the title compound at  $T^*=22$  K. The weakness of the relevant anomalies reflects presumably obvious  $Cu^{2+}$  ions and  $(VO)^{2+}$  units disorder in the system. It is supposed that the charge and geometry of the framework are controlled by the  $Cu^{2+}/(VO)^{2+}$  ratio; its variation may lead to a design of new materials.

© 2014 Elsevier Inc. All rights reserved.

## 1. Introduction

Vanadyl-phosphates have been a subject of interest for many decades because of their potential application as catalysts, ion conductors and sorbents. Representatives of this family with  $V^{4+}$  belong to the low-dimensional magnetic systems and can exhibit different types of magnetic ordering. Numerous vanadyl-diphosphates, namely  $M_2VOP_2O_7$  ( $M=Ag$ , Li, Rb, Cs, Na [1–5]),  $M(VO)_3(P_2O_7)_2$  ( $M=K$ , Sr, Pb, Ba [6–7]),  $M_2(VO)_3(P_2O_7)_2$  ( $M=Cs$ , Rb, K [8–9]),  $BaV_2P_2O_{10}$  [10] and  $M_2VO(P_2O_7)_2$  ( $M=V$ , Fe, Cr) [11] are known to be obtained in the system  $M$ –V(IV)–P–O. Their crystal structures are based on 2D or 3D mixed anionic frameworks formed from diphosphate groups and vanadium tetragonal pyramids and/or octahedra, sharing oxygen vertices. Currently, rather limited number of phosphate crystal structures simultaneously containing copper(II) and vanadium(IV) atoms has been investigated, i.e.  $CuV_2O_2(PO_4)_2$  [12],  $Rb_2Cu(VO_2)_2(PO_4)$  [2,13],  $CaCu(VO)(PO_4)_2$  and  $CaCu_{1.13}(VO)_{0.87}(PO_4)_2$  [14]. Two latter compounds were synthesized by solid state reactions and differ mainly by chemical ratio of copper and vanadium cations. Their crystal structures built particularly of planar  $CuO_4$ -squares and  $VO_{1+4}$  pyramids are characterized by

isomorphous  $Cu^{2+} \leftrightarrow VO^{2+}$  substitution. The phenomenon of  $Cu^{2+}$  replacement for  $V^{4+}$  is well known in cuprates, high-Tc superconductors [15,16].

Most of the above-mentioned vanadyl(IV)-phosphates were synthesized by solid-state and flux methods under vacuum. Our exploration of the system  $Cs$ – $V$ – $Cu$ – $P$ – $O$  in the air led to the synthesis of a first complex copper vanadium diphosphate with acentric novel type crystal structure reported here.

## 2. Experimental section

### 2.1. Synthesis and chemical composition

Single crystals of  $Cs_2Cu_{1+x}(VO)_{2-x}(P_2O_7)_2$ , ( $x=0.1$ ) were obtained by spontaneous crystallization from the melt in the system  $Cs$ – $Cu$ – $V$ – $P$ – $O$ . The starting agents were  $CsH_2PO_4$ ,  $CuO$  and  $V_2O_5$  taken in a molar ratio of 2:2:1. The reaction mixture was placed in the  $Al_2O_3$  crucible and heated to 850 °C, isothermed for 72 h and finally cooled to room temperature. Two phases obtained in a course of this experiment were mechanically extracted from a yellow transparent glass. The new compound was presented by green-bluish columnar crystals up to  $0.1 \times 0.3 \times 1.0$  mm of an amount estimated of 65% of the total yield. The second phase (~10%) was identified as transparent colorless isometric crystals

\* Corresponding author. Tel.: +7 495 9393850.

E-mail address: [lshvanskaya@mail.ru](mailto:lshvanskaya@mail.ru) (L. Shvanskaya).

of  $\alpha\text{-Cu}_2\text{P}_2\text{O}_7$  [17]. The presence of  $\text{V}^{4+}$  in the sample obtained may be explained by the fact that above 700 °C  $\text{V}_2\text{O}_5$  dissociates into  $\text{V}_2\text{O}_4$  and  $\text{O}_2$  [18] according to the following equations:



Thus, under the experimental condition we used, vanadium is likely to stay as  $\text{V}^{4+}$ .

Very small crystals of the title compound (as a minor phase) were also found in previous experiments of solid state reaction in the same system at 700 °C. A semi-quantitative X-ray spectral analysis (Leo 1429VP, energy-dispersive diffraction spectrometer INCA 350) of the phase showed the presence of Cs, Cu, V, P, and O atoms with an atomic ratio of Cu:V equal to 1.06:1.93 (result of 4 analyses) that is close to the ratio established by X-ray structural investigation.

## 2.2. Raman microspectroscopy

The Raman spectrum of a single crystal of the title compound was recorded using a confocal XPlora Raman microscope (Horiba Jobin-Yvon) in the range of 300–3000 cm<sup>-1</sup> with the exciting laser beam with wavelength of 532 nm. Each spectrum was accumulated in multi windows accumulation mode with 2 × 20 s exposure. Acquisition parameters (2400T grating, 300 μm hole, 100 μm slit, 100 × objective) provide laser spot size of ~1 μm and spectral resolution of ~3 cm<sup>-1</sup>.

## 2.3. X-ray analysis

The crystal structure of the title compound is found by single-crystal X-ray diffraction methods. The determination of unit cell parameters and data collection for the full Ewald sphere, were performed on a four-circle Xcalibur-S diffractometer equipped with CCD detector, using MoKα ( $\lambda=0.71073 \text{ \AA}$ ) radiation (graphite monochromator) at 298 K. The intensities were integrated and corrected for Lorentz and polarization effects. A numerical absorption correction was applied. Table 1 reports the crystallographic characteristics of the our phase and the experimental conditions of data collection and refinement. Atomic scattering curves and anomalous dispersion corrections were taken from the "International Tables for Crystallography" [19]. The crystal structure was solved via direct methods and refined against the F2 data using SHELX programs [20] in the framework of a Wingx32 software package [21].

Further details of the crystal structure investigation may be obtained from the Fachinformationszentrum Karlsruhe, 76344 Eggenstein-Leopoldshafen, Germany (fax: +49-7247-808-666; e-mail: crysdata@fiz-karlsruhe.de), on quoting the depository number CSD427933.

## 2.4. Magnetic and resonance measurements

Magnetic properties of  $\text{Cs}_2\text{Cu}_{1+x}(\text{VO})_{2-x}(\text{P}_2\text{O}_7)_2$ , (where  $x=0.1$ ) were measured by vibrating sample magnetometer (VSM) of Physical Properties Measurement System "Quantum Design" PPMS-9T in 2–300 K. Powder samples were obtained by crushing single crystals of the title compound in an agate mortar. Electron spin resonance (ESR) studies were carried out using an X-band ESR spectrometer CMS 8400 (ADANI) ( $f \approx 9.4 \text{ GHz}$ ,  $B \leq 0.7 \text{ T}$ ) equipped with a low temperature mount, operating in the range  $T=8\text{--}300 \text{ K}$ . The effective g-factor has been calculated with respect to a BDPA (a,g-bisdiphenylene-b-phenylallyl) reference sample with  $g_{\text{eff}}=2.00359$ .

## 3. Results and discussions

### 3.1. Raman spectra

The interpretation of Raman spectra was made on the basis of characteristic vibrations of  $\text{P}_2\text{O}_7$  group and vanadium polyhedra in comparison with structurally related vanadyl-diphosphates. In the Raman spectrum shown in Fig. 1, there are a number of strong bands assigned to the vibrations of  $\text{P}_2\text{O}_7$  groups. The most intense

**Table 1**  
Crystallographic data, experimental details and results of structure refinement.

Crystal data	
Formula, $M(\text{g/mol})$	$\text{Cs}_2\text{Cu}_{1.1}(\text{VO})_{1.9}(\text{P}_2\text{O}_7)_2$ , 810.79
Crystal system, space group	Orthorhombic, $Pn2_1/a$ (No. 33)
$a, b, c (\text{\AA})$	13.7364(2), 9.2666(2), 11.5678(2)
$V (\text{\AA}^3), Z$	1472.46(5), 4
$D_c (\text{g/cm}^3)$	3.657
Crystal size (mm <sup>3</sup> )	0.09 × 0.10 × 0.35
Crystal color	Green-bluish
Absorption coefficient $\mu (\text{mm}^{-1})$	8.148
Data collection	
Diffractometer	Xcalibur-S-CCD
Radiation, $\lambda (\text{\AA})$	MoKα, 0.71073, graphite monochromator
Temperature (K)	293(2)
Scan mode	$\omega$
Reflections collected	31196
$R_{\text{int}}, R_{\sigma}$	0.0516, 0.0296
$\theta_{\text{max}} (\text{°})$	30.0
$h, k, l$ range	$-19 \leq h \leq 19, -13 \leq k \leq 13, -16 \leq l \leq 16$
Refinement	
Program used to refine	SHELXL
Refinement method	Least-squares calculation on $F^2$
Independent/observed reflections	4292/3780
[ $I > 2\sigma(I)$ ]	239
Number of refined parameters	On the crystal shape
Correction for absorption	0.561, 0.246
$T_{\text{max}}, T_{\text{min}}$	$1/[b^2(Fo^2)+(0.0228P)^2]$ where $P=(Fo^2+2Fc^2)/3$
Weighting scheme	$R1=0.0295, wR_2=0.0600$
$R$ value [ $F_{\text{obs}} > 4\sigma(F_{\text{obs}})$ ]	$R1=0.0361, wR_2=0.0630$
$R$ value (all data)	1.068
GOF	Largest diff peak, hole/e ( $\text{\AA}^{-3}$ )
	0.838, -0.741

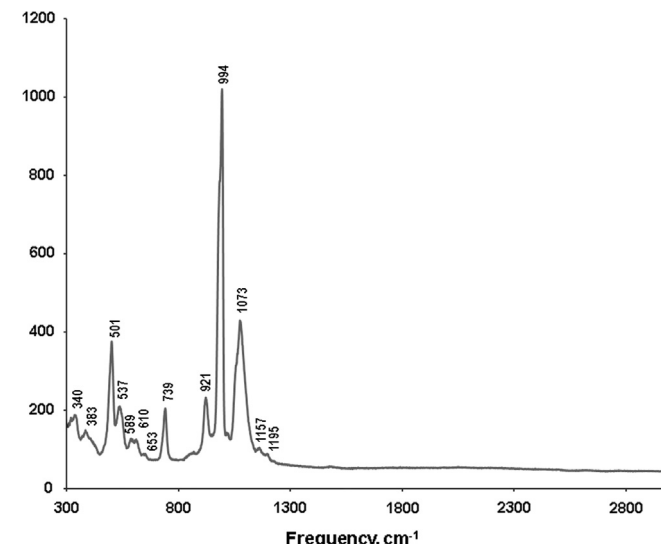


Fig. 1. Raman spectra of  $\text{Cs}_2\text{Cu}_{1+x}(\text{VO})_{2-x}(\text{P}_2\text{O}_7)_2$ .

peaks at 994, 1073 with the shoulder at 1055 cm<sup>-1</sup> are attributed to the symmetric stretching vibrations ( $\nu_s$  PO<sub>3</sub>) of P–O bonds in phosphate tetrahedra. Two weak bands at 1157 cm<sup>-1</sup> and 1195 cm<sup>-1</sup> are associated with  $\nu_{as}$  PO<sub>3</sub> vibrations. The bands of the P–O–P deformation vibrations with maximums at 340; 501 and 589 cm<sup>-1</sup> are assigned to the bridge ( $\delta$ POP) and P–O bonds ( $\delta$ PO<sub>3</sub>), respectively. Medium peak at 739 cm<sup>-1</sup> is associated with  $\nu_s$ (POP) mode. According to work [22] an intensity ratio of  $\nu_s$  P–O–P and  $\nu_s$  PO<sub>3</sub> can be considered as a criterion for the description of diphosphate group configuration. In our case this ratio is equal to 0.2 and points to an eclipsed configuration, which is in agreement with X-ray structure data.

An interpretation of V–O vibrations in the Raman spectra of vanadyl-diphosphates is tricky because corresponding modes appear in the region of the P–O bonds' vibration. As a rule, the symmetric stretching vibrations of the V–O and V=O bonds (in the VO<sub>5</sub> or VO<sub>5+1</sub> polyhedra) are attributed to the band in the region of 900–980 cm<sup>-1</sup> [22,23]. As has been shown in study [23] the  $\nu_s$  V=O mode frequency correlates with the interaction degree of the vanadium with apical oxygen atoms. Hence, the decreasing of the V=O distance values led to the lower V=O mode frequency. The peaks around 913, 926 and 978 cm<sup>-1</sup> were observed in the Raman spectra of Rb<sub>2</sub>(VO)<sub>3</sub>(P<sub>2</sub>O<sub>7</sub>)<sub>2</sub> (average distances V=O=1.592 Å) [22], (VO)<sub>2</sub>P<sub>2</sub>O<sub>7</sub> (av. V=O=1.598 Å) [23] and Cs<sub>2</sub>VOP<sub>2</sub>O<sub>7</sub> (V=O=1.606 Å) [22], respectively. In our case the average intense peak at 921 cm<sup>-1</sup> (average distances V=O=1.589 Å) can be attributed to the symmetric stretching vibration of the V=O bond. The symmetric stretching vibration peaks of the V–O bond appear at 653 and 610 cm<sup>-1</sup>. Finally, the weak peak observed at 383 cm<sup>-1</sup> can be attributed to the  $\delta$ VO<sub>2</sub> mode.

The results of Micro-Raman spectroscopic analysis indicate that studied phase presents an anhydrous compound, as no bands corresponding to OH-group vibration in the regions of 1250–1400 and 2300–3000 cm<sup>-1</sup> were found.

### 3.2. Structure refinement

The observed Laue symmetry and the systematic extinction conditions indicated the orthorhombic space groups *Pnma* and *Pn2<sub>1</sub>a*. The centrosymmetric space group *Pnma* was assumed initially, but the choice of the noncentrosymmetric space group *Pn2<sub>1</sub>a* (No. 33, standard setting *Pna2<sub>1</sub>*) has been confirmed in a course of crystal structure investigation. The sample under study was found to be a racemic twin with twinning parameter equal to 0.49(1). Final values of the atomic coordinates with equivalent isotropic displacement parameters and some selected bond lengths and angles are given in Tables 2 and 3, respectively. A bond-valence calculation has been performed using the algorithm and parameters from [24]; its results (see the Supplementary information, Table S1) clearly confirm the copper and vanadium valence state in the title compound.

As showed by our research, the crystal structure exhibits statistical disorder in distribution of cations and coordinated oxygen atoms. Thus, Cu1 and Cu2 atoms are both split in two positions with additional V1 and V2 at very short distances of 0.234(2) and 0.303(2) Å near copper atoms. Free refinement of the occupancy factors resulted in 0.461(9):0.539 for Cu1/V1 and 0.459(9):0.541 for Cu2/V2. The similar case of disordered Cu and V atoms in split positions was observed in the CaCu(VO)(PO<sub>4</sub>)<sub>2</sub> and CaCu<sub>1.13</sub>(VO)<sub>0.87</sub>(PO<sub>4</sub>)<sub>2</sub> crystal structures [14]. According to a disorder model including Cu1/V1 and Cu2/V2 atomic pairs, an oxygen atom O13 forming vanadyl bonds with V1 and V2, is also split in two positions with refined occupancy factors equal to 0.53(3):0.47. The occupancy factors of Cu1, Cu2, V1, V2, and O13 and O13' atoms were fixed in the final cycles of refinement to the idealized values of 1/2.

**Table 2**

Atomic coordinates and equivalent isotropic displacement parameters (Å<sup>2</sup>).

Atom	x(a)	y(b)	z(c)	<i>U</i> <sub>eq</sub>	occ
Cs1	0.12846(2)	0.61750(4)	0.26551(3)	0.0238(1)	1
Cs2	0.12325(2)	0.48060(4)	0.75103(3)	0.0244(1)	1
Cu1	0.38953(11)	0.6054(3)	0.43246(12)	0.018(2)*	0.5
V1	0.38840(16)	0.6086(3)	0.41239(17)	0.0118(2)*	0.5
Cu2	-0.13154(9)	0.6122(2)	0.43026(9)	0.0094(2)*	0.5
V2	-0.13232(12)	0.6148(3)	0.40417(13)	0.0094(2)*	0.5
V3	0.12379(7)	0.18477(12)	0.25744(9)	0.0136(3)	0.9
Cu3	0.1203(5)	0.2422(9)	0.2502(7)	0.0136(3)	0.1
P1	0.26897(7)	0.31853(12)	0.46800(10)	0.0122(3)	1
P2	0.02254(7)	0.81415(11)	0.54371(10)	0.0106(3)	1
P3	0.23680(7)	0.80909(12)	0.54795(10)	0.0109(3)	1
P4	0.47919(7)	0.29375(12)	0.45798(10)	0.0110(3)	1
O1	0.0298(2)	0.9769(3)	0.5498(4)	0.0227(13)	1
O2	0.2319(2)	0.9713(4)	0.5615(4)	0.0231(10)	1
O3	0.36953(18)	0.2416(3)	0.4326(3)	0.0166(9)	1
O4	0.1332(3)	0.0158(5)	0.2810(5)	0.0403(19)	1
O5	0.5035(2)	0.2551(3)	0.5830(3)	0.0145(10)	1
O6	0.12941(18)	0.7500(3)	0.5195(3)	0.0140(9)	1
O7	0.4861(2)	0.4523(3)	0.4313(3)	0.0207(10)	1
O8	0.2981(2)	0.7663(3)	0.4437(3)	0.0154(9)	1
O9	0.2653(2)	0.7354(4)	0.6596(3)	0.0253(10)	1
O10	-0.0374(2)	0.7674(3)	0.4402(3)	0.0150(9)	1
O11	0.2373(2)	0.2616(3)	0.5842(3)	0.0167(10)	1
O12	0.2864(3)	0.4778(4)	0.4720(4)	0.0421(16)	1
O13	0.3754(9)	0.604(2)	0.2760(6)	0.020(3)	0.5
O13'	0.3743(8)	0.611(2)	0.2324(6)	0.020(2)	0.5
O14	-0.0073(2)	0.7475(4)	0.6579(3)	0.0239(10)	1
O15	0.5415(2)	0.1978(3)	0.3811(3)	0.0194(10)	1
O16	0.1984(4)	0.3000(7)	0.3719(6)	0.026(2)	0.66
O16'	0.1969(10)	0.2282(13)	0.3918(13)	0.026(2)	0.34

\* Thermal parameters of the atoms refined in the isotropic approximation. The thermal parameters of the pairs atoms Cu1/V1; Cu2/V2; V3/Cu3 and O16/O16' were refined using the same value.

In addition to the same complementary population of Cu1/V1, Cu2/V2 and O13/O13' positions, V3 and Cu3 are also separated by a very short distance of 0.54(1) Å, preventing their simultaneous occupancy. The refinement has shown paired V3/Cu3 occupancy factors equal to 0.88(1):0.12. One more anionic position of O16 was found to be split in the structure with 0.66(1):0.34 occupancy ratio.

The crystal chemical formula of the vanadyl-diphosphate was recognized as Cs<sub>2</sub>[{(Cu<sub>0.5</sub><sup>+</sup>V<sub>0.5</sub><sup>+</sup>)<sub>2</sub>O][(V<sup>4+</sup>O)<sub>0.9</sub>Cu<sub>2.1</sub><sup>2+</sup>](P<sub>2</sub>O<sub>7</sub>)<sub>2</sub>. Idealized formula can be written as Cs<sub>2</sub>Cu<sub>1+x</sub>(VO)<sub>2-x</sub>(P<sub>2</sub>O<sub>7</sub>)<sub>2</sub>, where x=0.1.

### 3.3. Interatomic distances and crystal structure description

The cesium copper vanadyl-diphosphate forms an open anionic framework built up from Cu atoms in square pyramidal and square planar coordinations, VO<sub>5</sub> tetragonal pyramids and P<sub>2</sub>O<sub>7</sub> diphosphate groups, connected via Cu–O–V, Cu–O–P and V–O–P bonds, surrounding channels with extra-framework cesium cations. There are three crystallographically independent copper atoms in the unit cell, lying nearly in the centers of basal planes of square pyramids with bond lengths around Cu1 varying in the interval 1.942(4)–2.029(4) Å (average 1.957 Å). Around Cu2 these values change from 1.938(3) to 2.014(3) Å (average 1.936 Å), and cation–oxygen distances range from 1.850(10) to 1.951(16) Å in square planes around Cu3 with 10% occupancy. The additional apical oxygen atoms at distances of 2.324(7) and 2.388(7) Å from Cu1 and Cu2, respectively, complete their polyhedra, which therefore should be interpreted as square pyramids (CuO<sub>4+1</sub>) (Figs. 2 and 3). Each (from three symmetrically independent) tetravalent vanadium atom is coordinated by five oxygen atoms in a square pyramidal arrangement with one short V=O distance characteristic of a vanadyl group. These vanadyl bonds are as follows: V1=O13=1.588(7), V2=O13'=1.583(7) and V3=O4=1.595(5) Å. Four "equatorial" distances varied

**Table 3**  
Selected geometric parameters ( $\text{\AA}$ ,  $^\circ$ ).

Atom	Bond	Atom	Bond
$\text{Cs1O}_{10}$			
$\text{Cs1}-\text{O}5$	3.060(3)	$\text{Cs1}-\text{O}10$	3.347(3)
$\text{Cs1}-\text{O}11$	3.095(3)	$\text{Cs1}-\text{O}7$	3.368(4)
$\text{Cs1}-\text{O}6$	3.184(2)	$\text{Cs1}-\text{O}13$	3.397(12)
$\text{Cs1}-\text{O}1$	3.315(4)	$\text{Cs1}-\text{O}8$	3.403(3)
$\text{Cs1}-\text{O}16$	3.331(6)	$\text{Cs1}-\text{O}13'$	3.400(11)
$\text{Cs1}-\text{O}2$	3.397(4)	Average 3.290	
$\text{Cs2O}_{10}$			
$\text{Cs2}-\text{O}8$	3.175(3)	$\text{Cs2}-\text{O}5$	3.280(3)
$\text{Cs2}-\text{O}10$	3.192(3)	$\text{Cs2}-\text{O}4$	3.379(4)
$\text{Cs2}-\text{O}3$	3.205(3)	$\text{Cs2}-\text{O}15$	3.381(3)
$\text{Cs2}-\text{O}11$	3.209(3)	$\text{Cs2}-\text{O}13'$	3.343(20)
$\text{Cs2}-\text{O}14$	3.239(3)	$\text{Cs2}-\text{O}13$	3.499(19)
$\text{Cs2}-\text{O}9$	3.241(4)	Average 3.272	
$\text{CuO}_{4+2}$			
$\text{Cu}1-\text{O}7$	1.942(4)	$\text{Cu}1-\text{O}5$	2.029(4)
$\text{Cu}1-\text{O}8$	1.954(4)	$\text{Cu}1-\text{O}13'$	2.324(7)
$\text{Cu}1-\text{O}12$	1.901(5)		
$\text{V}1\text{O}_{1+4}$			
$\text{V}1-\text{O}13$	1.588(7)	$\text{V}1-\text{O}8$	1.951(4)
$\text{V}1-\text{O}7$	1.987(4)	$\text{V}1-\text{O}12$	1.977(5)
$\text{V}1-\text{O}5$	2.013(4)		
$\text{Cu}2\text{O}_{4+1}$			
$\text{Cu}2-\text{O}10$	1.938(3)	$\text{Cu}2-\text{O}11$	2.014(3)
$\text{Cu}2-\text{O}1$	1.892(3)	$\text{Cu}2-\text{O}13$	2.388(7)
$\text{Cu}2-\text{O}2$	1.901(4)		
$\text{V}2\text{O}_{1+4}$			
$\text{V}2-\text{O}13$	1.583(7)	$\text{V}2-\text{O}2$	1.949(4)
$\text{V}2-\text{O}10$	1.968(4)	$\text{V}2-\text{O}11$	1.987(4)
$\text{V}2-\text{O}1$	1.975(4)		
$\text{V}3\text{O}_{1+4}$			
$\text{V}3-\text{O}4$	1.595(5)	$\text{V}3-\text{O}14$	1.964(3)
$\text{V}3-\text{O}16'$	1.893(14)	$\text{V}3-\text{O}15$	1.966(3)
$\text{V}3-\text{O}9$	1.955(3)	$\text{V}3-\text{O}16$	1.986(6)
$\text{Cu}3\text{O}_4$			
$\text{Cu}3-\text{O}16$	1.850(10)	$\text{Cu}3-\text{O}15$	1.910(8)
$\text{Cu}3-\text{O}14$	1.882(8)	$\text{Cu}3-\text{O}16'$	1.951(16)
$\text{Cu}3-\text{O}9$	1.890(8)		
$\text{P}1\text{O}_4$			
$\text{P}1-\text{O}3$	1.608(3)	$\text{P}1-\text{O}16$	1.485(6)
$\text{P}1-\text{O}11$	1.508(4)	$\text{P}1-\text{O}16'$	1.568(14)
$\text{P}1-\text{O}12$	1.496(4)	Average 1.528	
$\text{P}2\text{O}_4$			
$\text{P}2-\text{O}1$	1.513(3)	$\text{P}2-\text{O}10$	1.516(3)
$\text{P}2-\text{O}6$	1.609(3)	$\text{P}2-\text{O}14$	1.515(4)
Average 1.538			
$\text{P}3\text{O}_4$			
$\text{P}3-\text{O}2$	1.513(4)	$\text{P}3-\text{O}8$	1.523(3)
$\text{P}3-\text{O}6$	1.608(3)	$\text{P}3-\text{O}9$	1.513(4)
Average 1.539			
$\text{P}4\text{O}_4$			
$\text{P}4-\text{O}3$	1.609(3)	$\text{P}4-\text{O}7$	1.504(3)
$\text{P}4-\text{O}5$	1.527(4)	$\text{P}4-\text{O}15$	1.520(3)
Average 1.540			
Atom	Bond angle	Atom	Bond angle
01-P2-P3-O2	3.3(2)	P3-O6-P2	132.5(2)
O7-P4-P1-O12	13.8(2)	P1-O3-P4	128.7(2)

from 1.987(4) to 2.013(4)  $\text{\AA}$  in the V1, change from 1.968(4) to 1.987(4)  $\text{\AA}$  in the V2, and lie in the interval 1.893(14)–1.986(6)  $\text{\AA}$  in the V3 polyhedra. Note that the  $\text{V}^{4+}$  cations are as usually displaced from the basal planes in the direction to the pyramidal vertices. In our structure this vanadium displacement corresponds to the distance between complementary positions of Cu and V atoms (Figs. 2 and 3).

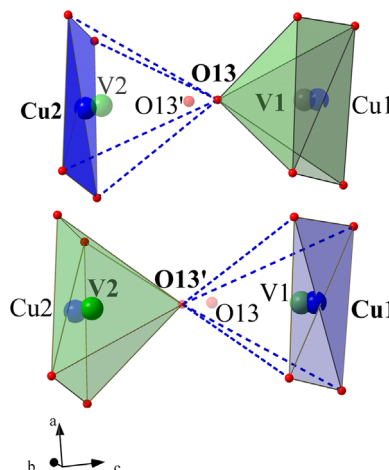


**Fig. 2.** Two possible alternative configurations of disordered Cu, V and O atoms in the crystal structure of  $\text{Cs}_2\text{Cu}_{1+x}(\text{VO})_{2-x}(\text{P}_2\text{O}_7)_2$ .

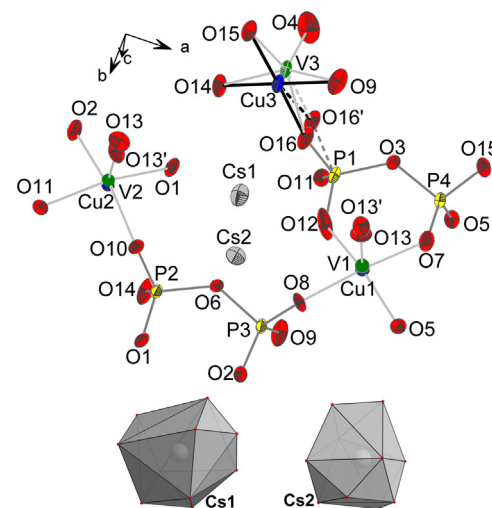


**Fig. 3.** The main structural elements of the title compound. Displacement ellipsoids are shown at the 60% probability level.

Four crystallographically independent P atoms in the structure are in a tetrahedral environment with average P–O distances equal to 1.528, 1.538, 1.539, and 1.540  $\text{\AA}$  for P1, P2, P3 and P4 position, respectively. The  $\text{PO}_4$  tetrahedra share oxygen atoms to form diphosphate  $\text{P}_2\text{O}_7$  groups. The P–O bridge distances in the diphosphate units are, as expected, longer than the terminal ones and exhibit values of 1.608(3)–1.609(3)  $\text{\AA}$  (Table 3). The both independent  $\text{P}_2\text{O}_7$  groups are characterized by an eclipsed conformation with O–P–P–O angles of 3.3(2) and 13.8(2) $^\circ$ . The P–O–P angles of the bridging bonds are equal to 132.5(2) $^\circ$  and to 128.7(2) $^\circ$ ; these values are close to generally observed.

The vanadium and copper square pyramids and diphosphate groups sharing vertices form cellular layers parallel to the ac plane (Fig. 4a). The adjacent along [0 1 0] layers with 4-, 6- and 8-membered rings, reproduced by a  $2_1$  screw axis, form a mixed anionic 3D-paraframework (Fig. 4b). The oxygen atom O4 forming vanadyl groups of the V3 polyhedron remains unshared with other polyhedra, and is pointed into the nine-membered rings (Fig. 5a). V3=O4 bonds are directed almost along the c axis, thus providing the polar character of the structure. The bonding between the layers occurs through corner-sharing oxygen atoms of the diphosphate groups of one layer and the Cu/V polyhedral of neighboring layers. The anionic paraframework described by the formula  $[\text{Cu}_{1+x}(\text{VO})_{2-x}(\text{P}_2\text{O}_7)_2]_{\infty\infty\infty}$  have a system of open channels running along

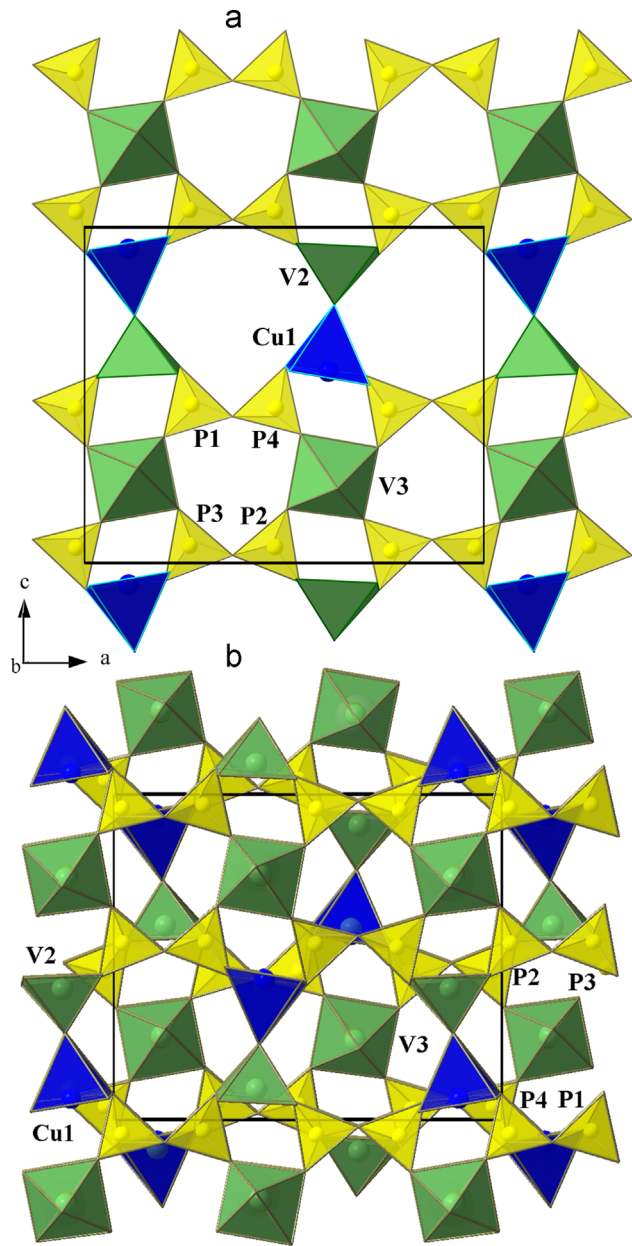


**Fig. 4.** The crystal structure of  $\text{Cs}_2\text{Cu}_{1+x}(\text{VO})_{2-x}(\text{P}_2\text{O}_7)_2$ . Shown in the (0 1 0) projection.

[0 0 1] and limited by 7-membered rings composed of Cu, V and P polyhedral (Fig. 6a). The cesium atoms located in the channels (Fig. 5) occupy two crystallographically independent positions with the  $\text{Cs}_1\text{O}$  and  $\text{Cs}_2\text{O}$  distances ranging from 3.060(3) to 3.403(3) and from 3.175(3) to 3.499(19) Å, respectively. The  $\text{Cs}_1$  and  $\text{Cs}_2$  atoms are surrounded by 10 oxygen atoms in their first coordination spheres (Fig. 3, bottom). It is worth mentioning that topologically identical structural fragment established in the composite solids  $\text{Cs}_2\text{Cu}_5(\text{P}_2\text{O}_7)_3 \cdot 3\text{CsCl}$ (I) and  $\text{Cs}_2\text{Cu}_7(\text{P}_2\text{O}_7)_4 \cdot 6\text{CsCl}$ (II) [25] can be recognized in our structure. The phases I and II belong to the class of hybrid materials based on a mixed open framework and templated by Cs–Cl salt [25]. The common for I and II network structure consists of sharing vertices  $\text{CuO}_4$  square-planers and  $\text{P}_2\text{O}_7$  groups as shown in Fig. 4b. Similar layers composed of  $\text{P}_2\text{O}_7$ ,  $\text{CuO}_4$  and  $\text{VO}_{1+x}$  polyhedra are extended along the (0 0 1) plane (Fig. 6a) in the title compound, where  $\text{VO}^{2+}$  substitute about one half of  $\text{Cu}^{2+}$ cations (Fig. 6). These complex layers are jointed into the 3D-framework

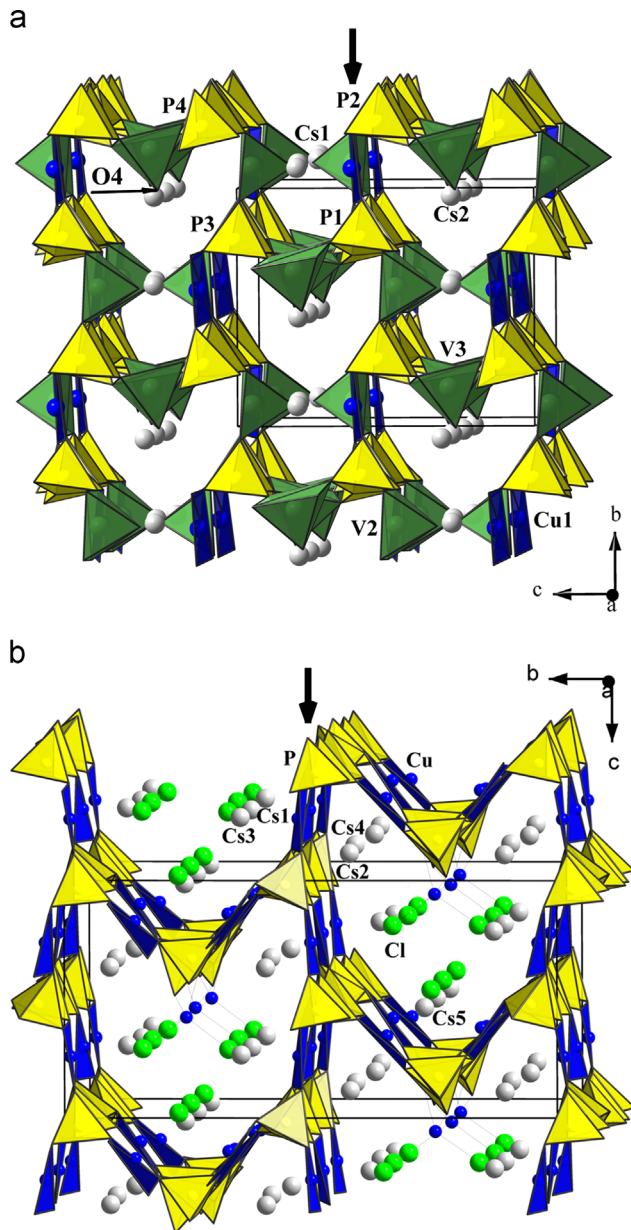


**Fig. 5.** Channels parallel to the [1 0 0] direction with cesium cations in the  $\text{Cs}_2\text{Cu}_{1+x}(\text{VO})_{2-x}(\text{P}_2\text{O}_7)_2$  (a) and in the  $\text{Cs}_2\text{Cu}_5(\text{P}_2\text{O}_7)_3 \cdot 3\text{CsCl}$  crystal structures. Similar structural fragments are indicated by thick arrows.

through  $\text{VO}_5$  oxo-complexes. Significantly more complicated structural fragments link similar Cu–P–O layers in I and II [25]. The distribution of cesium atoms in cavities formed around the identical structural fragments in three structures also demonstrates their similarity (Fig. 5). Close  $a$  and  $b$  unit cell parameters of three discussed structures reflect similar layer topologies, while different amount of Cs or Cs/CsCl templates directing the size and configuration of mixed open anionic framework, determine diverse values of the  $c$  parameters (Table 4).

The established  $x=0.1$  for our diphosphate,  $\text{Cs}_2\text{Cu}_{1+x}(\text{VO})_{2-x}(\text{P}_2\text{O}_7)_2$  reflects conditions of its synthesis. Based on the systematic features revealed for its crystal structure, we assume that different experimental conditions (e.g. oxygen pressure, etc.) may lead to the formation of a range of stoichiometric compounds with  $x$  equal to 0, 1 or 2. These hypothetical phases would have the following compositions:  $\text{Cs}_2\text{Cu}(\text{VO})_2(\text{P}_2\text{O}_7)_2$  with the highest possible vanadium and oxygen content,  $\text{Cs}_2\text{Cu}_2(\text{VO})(\text{P}_2\text{O}_7)_2$  with intermediate copper

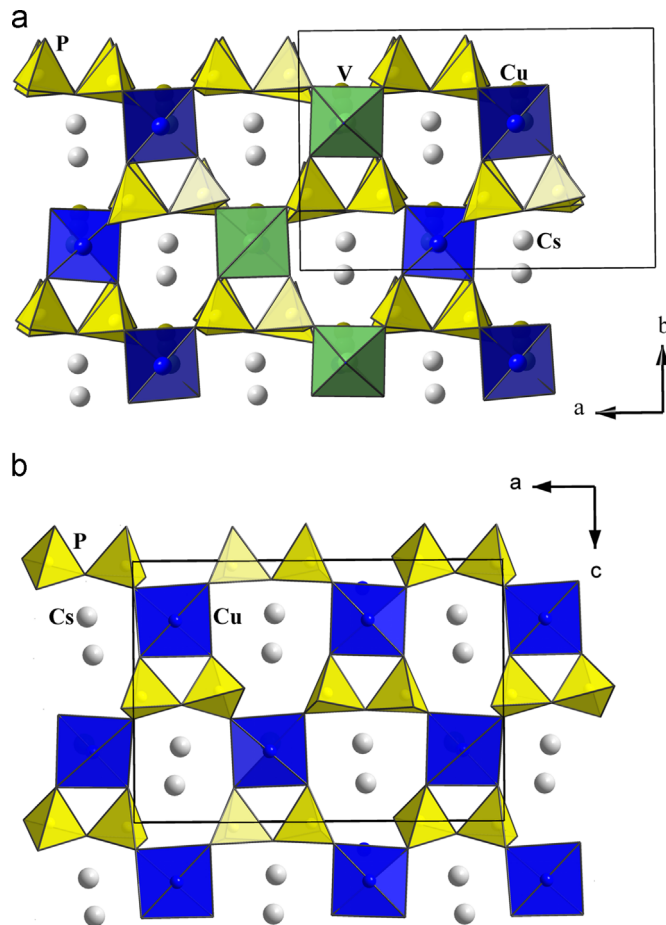


**Fig. 6.** Mixed anionic framework in the  $\text{Cs}_2\text{Cu}_{1+x}(\text{VO})_{2-x}(\text{P}_2\text{O}_7)_2$  crystal structure viewed along  $[0\ 0\ 1]$  (a); the Cu-P-O 2D network in the crystal structure of  $\text{Cs}_2\text{Cu}_5(\text{P}_2\text{O}_7)_3 \cdot 3\text{CsCl}$  (b).

amount, and a vanadium free  $\text{Cs}_2\text{Cu}_3(\text{P}_2\text{O}_7)_2$  formula, which characterizes a real compound also synthesized by flux method at lower temperature [26].

#### 3.4. Electron spin resonance

Evolution of the ESR spectra in a powder sample of  $\text{Cs}_2\text{Cu}_{1+x}(\text{VO})_{2-x}(\text{P}_2\text{O}_7)_2$  ( $x=0.1$ ) with temperature is shown on Fig. 7. The whole spectrum is dominated by an absorption line of Lorentzian lineshape indicative of exchange narrowing. Nevertheless, an accurate quantitative analysis of the lineshape requires using of two Lorentzian functions for proper description of experimental data. It means that two resonance modes may be distinguished in the spectrum. To evaluate the main ESR parameters of these two components the experimental spectra have been fitted by sum of two Lorentzian functions:

$$\frac{dP}{dB} \propto \frac{d}{dB} \left[ \frac{\Delta B}{\Delta B^2 + (B - B_r)^2} \right] \quad (2)$$

where  $P$  is the power absorbed in the ESR experiment,  $B$ —magnetic field,  $B_r$ —resonance field,  $\Delta B$ —the linewidth. Apparently the fitted curves (red solid lines in Fig. 7a) agree well with experimental data. Representative example of the spectrum decomposition is given in Fig. 7b: resolved resonance modes are denoted by colored dashed lines, while their sum is shown by red solid line. The values of g-factor obtained for two resolved components at room temperature are on average  $g_1=2.001$  and  $g_2=2.037$ . Since two paramagnetic

**Table 4**

Crystallographic characteristics of complex diphosphates crystal structures containing the topologically identical fragments.

Parameters	Compound
$a$	$\text{Cs}_2\text{Cu}_{1+x}(\text{VO})_{2-x}(\text{P}_2\text{O}_7)_2$
$b$	$\text{Cs}_2\text{Cu}_5(\text{P}_2\text{O}_7)_3 \cdot 3\text{CsCl}^*$
$c$ (Å)	$\text{Cs}_2\text{Cu}_7(\text{P}_2\text{O}_7)_4 \cdot 6\text{CsCl}^*$
$V$ (Å <sup>3</sup> )	
S. G.	

\* The unit cell parameters are reduced to the system accepted for the  $\text{Cs}_2\text{Cu}_{1+x}(\text{VO})_{2-x}(\text{P}_2\text{O}_7)_2$  crystal structure.

ions  $\text{Cu}^{2+}$  ( $d^9$ ,  $S=1/2$ ) and  $\text{V}^{4+}$  ( $d^1$ ,  $S=1/2$ ) present in the sample under study it would be quite naturally to expect the presence of two resonance modes in ESR spectrum. Taking into account the crystal structure data, note that the ESR absorption signal in powder sample of  $\text{Cs}_2\text{Cu}_{1+x}(\text{VO})_{2-x}(\text{P}_2\text{O}_7)_2$  ( $x=0.1$ ) is a statistical average over the presumably anisotropic spectra with regard to the orthorhombic crystal axes and the existence of three crystallographically nonequivalent sites for the pairs atoms Cu1/V1; Cu2/V2; V3/Cu3, which are coordinated by four/five oxygen atoms in square planar/square pyramidal arrangement and forming  $n$ -membered rings composed of Cu, V and P polyhedra. Presumably, two modes may be assigned to two exchange-narrowed lines reflecting the signals from  $\text{Cu}^{2+}$  and  $\text{V}^{4+}$  paramagnetic centers, which interact with each other. Both  $d^1$  and  $d^9$  ions have  $t_{2g}e_g$  configuration and if neglecting tetragonal or trigonal distortion effects, the crystal field of octahedral or tetrahedral symmetry splits this state into triplet  $\Gamma_5$  and doublet  $\Gamma_3$  states but the order of these energy levels is opposite for two configurations. In this case the principal values for g-tensor are [27]:

$$g_{||} = g_{zz} = \frac{g_e - 8\lambda}{\Delta} \quad (3)$$

$$g_{\perp} = g_{xx} = g_{yy} = \frac{g_e - 2\lambda}{\Delta},$$

or in isotropic case:

$$g = g_{zz} = g_{xx} = g_{yy} = \frac{g_e - 4\lambda}{\Delta} \quad (4)$$

where  $g_e$  is a free electron g-value,  $\lambda$  is a spin-orbital coupling constant and  $\Delta$  is the crystal field energy splitting. Typically  $\lambda > 0$  for  $d^1$  ions, while  $\lambda < 0$  for  $d^9$  ions, hence one should expect that  $g < g_e$  and  $g > g_e$  for  $d^1$  and  $d^9$  ions, correspondingly. At the same time, it is apparent that both values of g-factor obtained for two resolved components differ noticeably from typical values observed for  $\text{V}^{4+}$  and  $\text{Cu}^{2+}$  compounds, which are usually ranged as  $g=1.93-1.98$  [28–35] and  $g=2.02-2.22$  [36–43] in pyramidal, square planar or octahedral oxygen coordination for  $\text{V}^{4+}$  and  $\text{Cu}^{2+}$  correspondingly. If the value of  $g_2$  could be more or less reasonably assigned to the signal from  $\text{Cu}^{2+}$  ions, the reduction of negative shift for the value of  $g_1$  compared to the free electron g-value indicates either strong covalence effect for  $\text{V}^{4+}$  ions subsystem or important role of exchange spin-spin interactions between Cu and V subsystems. Indeed, in the latter case when both fine and hyperfine structures expected either from natural  $^{63}\text{Cu}$  and  $^{65}\text{Cu}$  ( $I=3/2$ ) or  $^{51}\text{V}$  ( $I=7/2$ ) isotopes were not resolved in experimental spectra our data may be interpreted as follows. In first order perturbation theory Spin-Hamiltonian for two different  $S=1/2$  spins  $i$  and  $j$  (with different g-factors) with isotropic interaction  $\mathfrak{H}$  may be written as [44]:

$$\mathcal{H} = \beta H_z (g_{iz} S_{iz} + g_{jz} S_{jz}) + \mathfrak{H}(S_i \times S_j) \quad (5)$$

where  $H_z$  is magnetic field applied along z-axis, which corresponds to main axis of both g-tensors,  $\mu_B$  is Bohr magneton. In absence of the interaction between spins  $i$  and  $j$  (similarly to case of the isolated

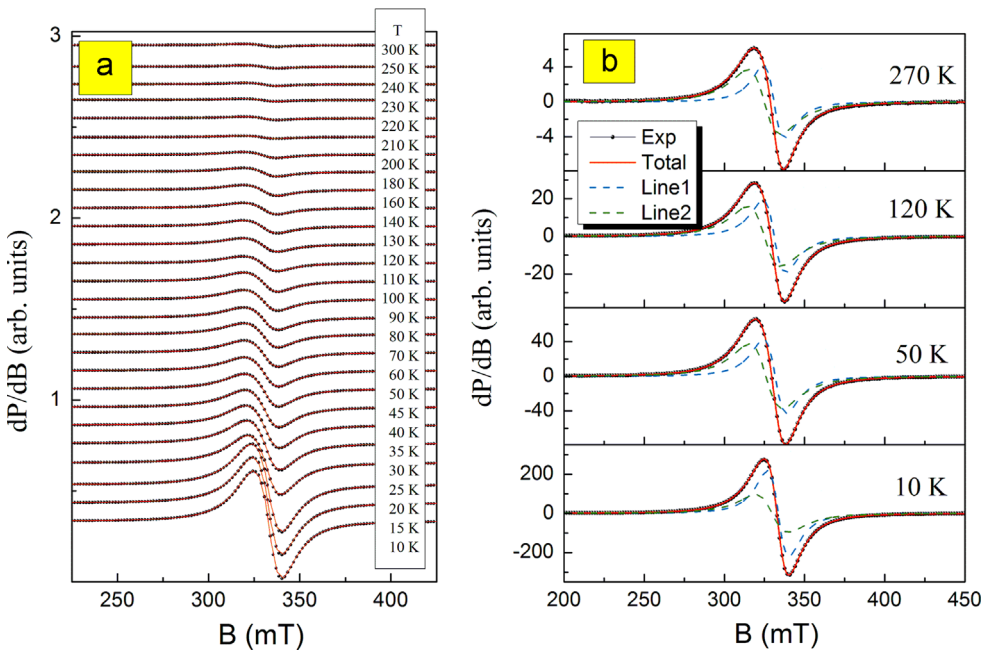


**Fig. 7.** Evolution of the ESR spectra of powder sample  $\text{Cs}_2\text{Cu}_{1+x}(\text{VO})_{2-x}(\text{P}_2\text{O}_7)_2$  with temperature: experimental data are shown by circles, their analysis in accordance with sum of two Lorentzian profiles are shown by lines, blue and green dashed lines represent two resolved components and red solid line is their sum. (For interpretation of the references to color in this figure legend, the reader is referred to the web version of this article.)

ions) the transitions occur at  $h\nu=g_{iz}\mu_B H_z$  and  $h\nu=g_{jz}\mu_B H_z$  (as schematically shown in Fig. 8). When the interaction is small enough two doublets ( $|++>\leftrightarrow|-+>$ ;  $|-->\leftrightarrow|+->$  and  $|++>\leftrightarrow|+->$ ;  $|-->\leftrightarrow|-+>$ ) are observed for these allowed transitions and the separation between branches in each doublet is equal to  $\mathfrak{J}$  in the first approximation. With increasing the exchange interaction  $\mathfrak{J}$  the outside transitions ( $|++>\leftrightarrow|-+>$  and  $|-->\leftrightarrow|-+>$ ) are diverged and weakened, while inside transitions ( $|-->\leftrightarrow|+->$  and  $|++>\leftrightarrow|+->$ ) shifts to the central frequency  $h\nu=1/2(g_{iz}+g_{jz})\mu_B H_z$  and their intensity increases considerably, so that at certain exchange parameter only these two branches may be observed in the spectra (see Fig. 8). Obviously, in such a case the values of effective g-factors may adopt the values, which are noticeably shifted according to those predicted from crystal field theory for given ligand coordination.

Temperature dependencies of the ESR linewidth, effective g-factor for two resolved components of ESR spectra and the integral ESR intensity derived from the fitting are collected in Fig. 9. Both the ESR linewidth and effective g-factor remain almost constant over the whole temperature range investigated and consistently vary with temperature showing slight deviation of g-factor from high-temperature values below  $\sim 50$  K, which may reflects to development of short-range correlations in the system under study. This similarity in behavior of two paramagnetic subsystems (Cu and V ones) corroborates well with our interpretation assuming noticeable exchange interaction between copper and vanadium spin subsystems in the title compound. The integral ESR intensity, which proportional to the number of magnetic spins, was calculated by double integration of experimental derivative curve. Note, that the  $\Delta B_1$  linewidth presents clear kink at  $T^*\sim 22$  K. Obviously, it is in consistence with static susceptibility data  $\chi(T)$  presented below.

### 3.5. Magnetization

The temperature dependence of magnetic susceptibility of  $\text{Cs}_2\text{Cu}_{1+x}(\text{VO})_{2-x}(\text{P}_2\text{O}_7)_2$  ( $x=0.1$ ) is shown in Fig. 10. It demonstrates Curie–Weiss–like behavior in the whole studied temperature range. The fit of experimental data in the range 150–300 K

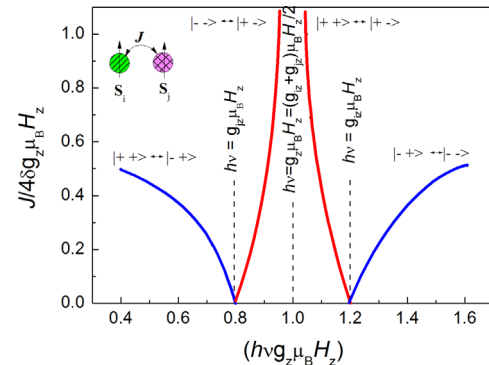


**Fig. 8.** Spectrum of pair of the different ions  $i$  and  $j$  (with different g-factors) coupled by an isotropic interaction  $\mathfrak{J}$ , which is described by Hamiltonian (Eq. (5)) when the difference between Zeeman energy  $h\nu=1/2(g_{iz}+g_{jz})\mu_B H_z=2\delta g_z\mu_B H_z$  is relatively large, compared to exchange parameter  $\mathfrak{J}$ . The diagram is constructed for the case  $\delta g_z/g_z=0.2$ .

with the function

$$\chi=\chi_0+\frac{C}{(T-\Theta)} \quad (6)$$

allows estimating temperature independent term to be equal to  $\chi_0=-4.07\times 10^{-4}$  emu/mol, Curie constant  $C=1.08$  emu K/mol and Weiss temperature  $\Theta=-14$  K. Experimental data presented in the inset in  $(\chi-\chi_0)(T-\Theta)$  vs.  $T$  scale indicate rather weak anomaly at  $T^*=22$  K. Moreover, this scale allows unveiling the predominance of  $\chi(T)$  dependence over Curie–Weiss law at low temperatures. The experimentally obtained  $\chi_0$  is close to the sum of partial diamagnetic contributions from ions in the compound  $\text{Cs}_2\text{Cu}_{1+x}(\text{VO})_{2-x}(\text{P}_2\text{O}_7)_2$  ( $x=0.1$ ) which amounts  $-2.91\times 10^{-4}$  emu/mol [45]. Obtained Curie constant allows estimating the effective magnetic moment

$$\mu_{\text{eff}}^2=\frac{3k_B C}{N_A} \quad (7)$$

as  $\mu_{\text{eff}}^2=8.64\mu_B^2$ , where  $k_B$  and  $N_A$  are Boltzmann and Avogadro constants. This value can be compared with that calculated by the

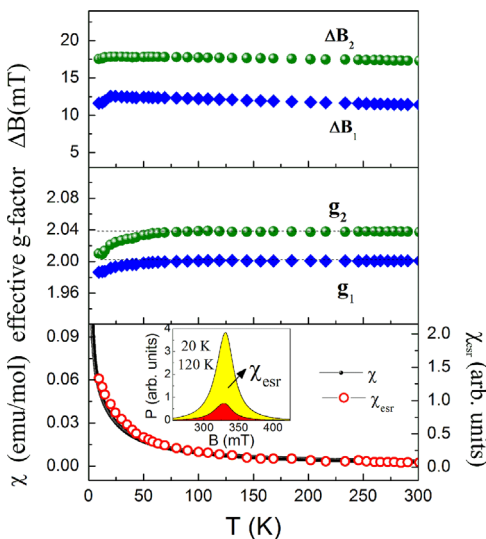


**Fig. 9.** The temperature dependences of the ESR linewidth for two resolved components of ESR spectra (upper panel), principal values of g-tensor (middle panel) and the integral ESR intensity (lower panel) for  $\text{Cs}_2\text{Cu}_{1+x}(\text{VO})_{2-x}(\text{P}_2\text{O}_7)_2$ .

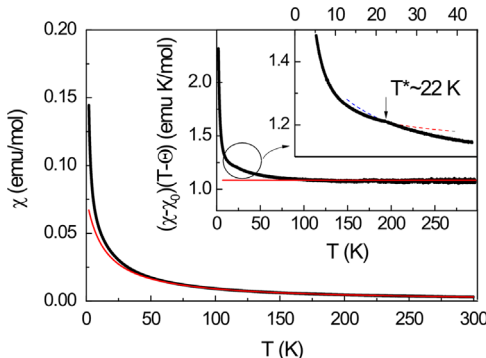


**Fig. 10.** The temperature dependence of magnetic susceptibility of  $\text{Cs}_2\text{Cu}_{1+x}(\text{VO})_{2-x}(\text{P}_2\text{O}_7)_2$  measured under 0.1 T magnetic field. Thick and thin lines are experimental points and Curie-Weiss fit. The inset represents the same dependence in  $(\chi - \chi_0)(T - \Theta)$  vs. T scale. Dashed dotted lines are the guides for an eye to highlight the  $T^*$  anomaly.

formula

$$\mu_{\text{eff}}^2 = \mu_{\text{eff}}^2 \sum_i n_i g_i^2 S_i (S_i + 1) \mu_B^2 \quad (8)$$

for  $n_i$  magnetic ions per formula unit with  $g$ -factors  $g_i$  and spin magnetic moment  $S_i$ . ESR data gives the  $g$ -factors for  $\text{Cu}^{2+}$  ( $S=1/2$ ) and  $\text{V}^{4+}$  ( $S=1/2$ ) ions as  $g_{\text{Cu}}=2.037$  and  $g_{\text{V}}=2.001$ . Thus, effective moment can be estimated as  $9.13 \mu_B^2$  which corresponds to the experimental value  $8.64 \mu_B^2$ . The negative Weiss temperature  $\Theta=-14$  K indicates the predominance of antiferromagnetic exchange interactions at high temperatures while low-temperature upturn in  $\chi(T)$  curve signals the appearance of weaker ferromagnetic exchange interactions.

The  $\text{Cu}^{2+}$  ions in square oxygen coordination and  $\text{V}^{4+}$  ions in square pyramidal coordination possess magnetically active  $d_{x^2-y^2}$  and  $d_{xy}$  orbitals in basal plane [46]. Thus the only direct Cu-O-V bond in the structure directed perpendicular to the basal plane is not important for magnetic exchange. These magnetically active orbitals may participate in magnetic exchange interactions via phosphate groups [47]. The origin of the appearance of ferromagnetic component in exchange interactions in  $\text{Cs}_2\text{Cu}_{1+x}(\text{VO})_{2-x}(\text{P}_2\text{O}_7)_2$  ( $x=0.1$ ) can be found in closely packed vanadyl pyramids for V1 and V3 ions which are placed in 4.06 Å from each other. In Ref. [48] the

possibility of ferromagnetic exchange interaction was shown for vanadyl pyramids separated by 4.5 Å and such exchange was weakened with the increase of separating distance and even changed the sign for the antiferromagnetic one. The exchange interaction between other vanadium and copper ions can be assumed most probably antiferromagnetic [49,50]. Partial chemical disorder, i.e. mixed occupancy of Cu1/V1, Cu2/V2, Cu3/V3 positions may induce the appearance of exchange interactions bands which weakens the anomaly at  $T^*=22$  K corresponding to magnetic order formation. The presence of multiple ferro/antiferromagnetic exchange interactions in  $\text{Cs}_2\text{Cu}_{1+x}(\text{VO})_{2-x}(\text{P}_2\text{O}_7)_2$  ( $x=0.1$ ) structure and its partial disorder may result in cluster-glass-like features of magnetic state below  $T^*$ .

#### 4. Conclusions

The novel cesium copper vanadyl-diphosphate containing simultaneously  $\text{Cu}^{2+}$  and  $(\text{VO})^{2+}$  cations has been obtained from the melt. Our data has confirmed a possibility of high-temperature  $\text{Cu}^{2+} \leftrightarrow (\text{VO})^{2+}$  substitution, which is fruitful for crystal structure design of new open framework compounds. This effect is of crucial importance for the magnetic superexchange interaction. Instead of well defined exchange interaction parameters naturally expected for a regular system a spread of these quantities is realized presumably in  $\text{Cs}_2\text{Cu}_{1+x}(\text{VO})_{2-x}(\text{P}_2\text{O}_7)_2$  ( $x=0.1$ ). As a result, the relatively dense magnetic subsystem presents exclusively weak anomaly at cluster-glass formation temperature. Rather small available amount of the title compound prevented studies of ac-susceptibility, specific heat and dielectric permittivity which will be naturally next steps in its deep characterization.

#### Acknowledgments

We thank V.O. Yapaskurt for the X-ray spectral analysis of the crystals and N.V. Zubkova for the X-ray experiment. This work was supported in part from the Ministry of Education and Science of the Russian Federation in the framework of Increase Competitiveness Program of NUST "MISiS" (No. K2-2014-036), by the Russian Foundation for Basic Research projects 13-02-00174, 14-02-00111, 14-02-92002 and by the grants-in-aid of Ministry of Education and Science of Russia MK-7138.2013.2. V.D. Shcherbakov acknowledges support from M.V. Lomonosov Moscow State University Program of Development. The acknowledgements come at the end of an article after the conclusions and before the notes and references.

#### Appendix A. Supporting information

Supplementary data associated with this article can be found in the online version at <http://dx.doi.org/10.1016/j.jssc.2014.11.004>.

#### References

- [1] A. Daidouh, M.L. Veiga, C. Pico, J. Solid. State Chem. 130 (1997) 28–34.
- [2] M.S. Kishore, V. Pralong, V. Caignaert, U.V. Varadaraju, B. Raveau, Solid State Sci. 10 (2008) 1285–1291.
- [3] K.H. Lii, S.L. Wang, J. Solid State Chem. 82 (1989) 239–246.
- [4] A. Daidouh, M.L. Veiga, C. Pico, Solid State Ionics 106 (1998) 103–112.
- [5] L. Benhamada, A. Grandin, M.M. Borel, A. Leclaire, B. Raveau, J. Solid State Chem. 101 (1992) 154–160.
- [6] L. Benhamada, A. Grandin, M.M. Borel, A. Leclaire, B. Raveau, J. Solid State Chem. 97 (1992) 131–140.
- [7] M.M. Borel, M. Hervieu, A. Leclaire, C. Michel, J. Chardon, J. Provost, B. Raveau, Chem. Mater. 11 (1999) 3655–3665.
- [8] K.H. Lii, S.L. Wang, J. Solid State Chem. 80 (1989) 127–132.
- [9] A. Leclaire, H. Chahboun, D. Grout, B. Raveau, J. Solid State Chem. 77 (1988) 170–179.

- [10] A. Grandin, J. Chardon, M.M. Borel, A. Leclaire, B. Raveau, *J. Solid State Chem.* 9 (1992) 297–302.
- [11] R. Glaum, E. Benser, H. Hibst, *Chem. Ing. Tech.* 79 (2007) 843–850 (6).
- [12] E. Benser, M. Schönebornnund, R. Glaum, Z. Anorg. Allg. Chem. 634 (2008) 1677–1686.
- [13] O. Yakubovich, I. Steel, O. Dimitrova, *Acta Crystallogr., Sect. C: Cryst. Struct. Commun.* 64 (2008) i62–i65.
- [14] S. Meyer, H.k. Muller-Buschbaum, Z. Naturforsch. 53 (1998) 521–526.
- [15] L. Liu, G. Che, G. Liu, C. Dong, H. Chen, S. Jia, Y. Ni, Z. Zhao, *Physics C* 384 (2003) 75–80.
- [16] E.Z. Kurmaev, A. Moewes, G.T. Woods, T.A. Callcott, N.D. Zhigadlo, E. Takayama-Muromachi, V.R. Galakhov, D.L. Ederer, *J. Solid State Chem.* 170 (2003) 188–191.
- [17] H. Effenberger, *Acta Crystallogr., Sect. C: Cryst. Struct. Commun.* 46 (1990) 691–692.
- [18] R.J.H. Clark, *The Chemistry of Titanium and Vanadium*, Elsevier, Amsterdam, The Netherlands, 1968.
- [19] E. Prince, *International Tables for Crystallography*, third ed., Kluwer, Dordrecht, The Netherlands, 2004 (Tables 4.2.6.8 and 6.1.14).
- [20] G.M. Sheldrick, *Acta Crystallogr., Sect. A: Found. Crystallogr.* 64 (2008) 112–122.
- [21] L.J. Farrugia, *J. Appl. Crystallogr.* 32 (1999) 837–838.
- [22] V.P. Mahadevan Pillai, B.R. Thomas, V.U. Nayar, K.-H. Lii, *Spectrochim. Acta, Part A: Mol. Biomol. Spectrosc.* 55 (1999) 1809–1817.
- [23] U. Kuhlmann, C. Thomsen, A.V. Prokofiev, F. Bullesfeld, E. Uhrig, W. Assmus, *Physics C* 301 (2001) 276–285.
- [24] D. Braun, D. Altermatt, *Acta Crystallogr., Sect. B: Struct. Sci.* 41 (1985) 244–247.
- [25] Q. Huang, S.-J. Hwu, *Inorg. Chem.* 42 (2003) 655–657.
- [26] K.G.S. Ramamohotti, X. Mo, M. Kirklyn, S.-J. Hwu, *Inorg. Chem.* 45 (2006) 3665–3670.
- [27] J.E. Wertz, J.R. Bolton, *Electron spin resonance, Elementary Theory and Practical Applications*, McGraw-Hill Book Company, New York, NY, 1972.
- [28] J.V. Choukroun, A. Pashchenko, Y. Ksari, J.Y. Henry, F. Mila, P. Millet, P. Monod, A. Stepanov, J. Dumas, R. Buder, *Eur. Phys. J. B: Condens. Matter Complex Syst.* 14 (2000) 655–659.
- [29] V.A. Pashchenko, A. Sulpice, F. Mila, P. Millet, A. Stepanov, P. Wyder, *Eur. Phys. J. B: Condens. Matter Complex Syst.* 21 (2001) 473–476.
- [30] F. Chabre, A.M. Ghorayeb, P. Millet, V. Pashchenko, A. Stepanov, *Phys. Rev. B: Condens. Matter* 72 (2005) 012415.
- [31] J. Deisenhofer, S. Schaile, J. Teyssier, Z.h.e. Wang, M. Hemmida, H.-A. Krug von Nidda, R.M. Eremina, M.V. Eremin, R. Viennois, E. Giannini, D. Marel, A. Loidl, *Phys. Rev. B: Condens. Matter* 86 (2012) 214417.
- [32] V.A. Ivanshin, V. Yushankhai, J. Sichelschmidt, D.V. Zakharov, E.E. Kaul, C. Geibel, *Phys. Rev. B: Condens. Matter* 68 (2003) 064404.
- [33] A. Vasiliev, O. Volkova, E. Zvereva, M. Isobe, Y. Ueda, S. Yoshii, H. Nojiri, V. Mazurenko, M. Valentyuk, V. Anisimov, L. Solovyev, R. Klingeler, B. Büchner, *Phys. Rev. B: Condens. Matter* 87 (2013) 134412.
- [34] S.K. Misra, J.-S. Sun, *Phys. Rev. B: Condens. Matter* 42 (1990) 8601–8604.
- [35] V.K. Jain, N.V. Vugman, V.S. Yadav, *Phys. Rev. B: Condens. Matter* 37 (1988) 9716–9718.
- [36] R.M. Krishna, S.K. Gupta, *Bull. Magn. Resonance* 16 (1994) 239–291.
- [37] L. Shvanskaya, O. Yakubovich, A. Ivanova, S. Baidya, T. Saha-Dasgupta, E. Zvereva, A. Golovanov, O. Volkova, A. Vasiliev, *New J. Chem.* 37 (2013) 2743–2750.
- [38] V. Kataev, K.-Y. Choi, M. Grüninger, U. Ammerahl, B. Büchner, A. Freimuth, A. Revcolevschi, *Phys. Rev. Lett.* 86 (2001) 2882–2885.
- [39] A. Zorko, D. Arčon, H. van Tol, L.C. Brunel, H. Kageyama, *Phys. Rev. B: Condens. Matter* 69 (2004) 174420.
- [40] Y.C. Arango, E. Vavilova, M. Abdel-Hafiez, O. Janson, A.A. Tsirlin, H. Rosner, S.-L. Drechsler, M. Weil, G. Nénert, R. Klingeler, O. Volkova, A. Vasiliev, V. Kataev, B. Büchner, *Phys. Rev. B: Condens. Matter* 84 (2011) 134430.
- [41] A. Zorko, F. Bert, A. Ozarowski, J. van Tol, D. Boldrin, A.S. Wills, P. Mendels, *Phys. Rev. B: Condens. Matter* 88 (2013) 144419.
- [42] A.U.B. Wolter, F. Lipps, M. Schäpers, S.-L. Drechsler, S. Nishimoto, R. Vogel, V. Kataev, B. Büchner, H. Rosner, M. Schmitt, M. Uhlzar, Y. Skourski, J. Wosnitza, S. Stollow, K.C. Rule, *Phys. Rev. B: Condens. Matter* 85 (2012) 014407.
- [43] J.M. Law, P. Reuvekamp, R. Glaum, C. Lee, J. Kang, M.-H. Whangbo, R.K. Kremer, *Phys. Rev. B: Condens. Matter* 84 (2011) 014426.
- [44] A. Abragam, B. Bleaney, *Electron Paramagnetic Resonance of Transition Ions*, Clarendon Press, Oxford, 1970.
- [45] G.A. Bain, J.F. Berry, *J. Chem. Educ.* 85 (2008) 532–536.
- [46] V.A. Korotin, Ph.D. Thesis, Ekaterinburg, 2003.
- [47] G.S. Uhrig, B. Normand, *Phys. Rev. B: Condens. Matter* 63 (2001) 134418.
- [48] A.A. Tsirlin, R. Nath, A.M. Abakumov, R.V. Shpanchenko, C. Geibel, H. Rosner, *Phys. Rev. B: Condens. Matter* 81 (2010) 174424.
- [49] R.P. Dole, T. Bauer, M. Julve, F. Lloret, J. Cano, M. Nieuwenhuyzen, P.E. Kruger, *Dalton Trans.* 44 (2007) 5140–5147.
- [50] D. Venegas-Yazigi, K. Mucoz-Becerra, E. Spodine, K. Brown, C. Aliaga, V. Paredes-Garcha, P. Aguirre, A. Vega, R. Cardoso-Gil, W. Schnelle, R. Kniep, *Polyhedron* 29 (2010) 2426–2434.